243004: garnet-bearing pelitic schist, Top Up Rise prospect

(*Basement to Canning Basin, North Australian Craton*)

Kelsey, DE, Korhonen, FJ, Romano, SS and Spaggiari, CV

Location and sampling

Wilson (SF 52-9), Top Up Rise (4352)

MGA Zone 52, 338397E 7503072N

WAROX site CVSWAO000004

Sampled on 14 June 2019

This sample was collected from the 234.67 – 234.82 m depth interval of diamond drillcore TUR13DD004, drilled in 2013 by Border Exploration Pty Ltd at their Top Up Rise prospect (Marshall, 2013), with support from the Western Australian Government's Exploration Incentive Scheme (EIS). The drillhole is located about 40 km northwest of Kiwirrkurra community, 30 km northeast of Top Up Rise, and 26 km north-northwest of the Pollock Hills.

Geological context

The unit sampled is a garnet-bearing micaceous schist within crystalline basement beneath the southeastern margin of the Canning Basin, about 20 km west of the exposed Aileron Province of the North Australian Craton. On the basis of detrital zircon age data the basement rocks at the Top Up Rise prospect are likely part of the Aileron Province of the North Australian Craton (Kelsey et al., 2022). The Top Up Rise prospect is located above a distinct northeast-trending gravity anomaly bounded by northeast-trending shear zones (Marshall, 2013; Kelsey et al., 2022). Five co-funded EIS diamond drillcores from Top Up Rise contain partially melted or melt-injected upper-amphibolite to low-granulite facies basement rocks. SHRIMP U–Pb zircon geochronology of several granitic gneiss samples has so far revealed a major age peak at c. 1875 Ma, which is distinctly older than known magmatic rocks in the Aileron and Warumpi Provinces (Scrimgeour, 2013a,b), but comparable to a major detrital zircon age peak from Paleoproterozoic metasedimentary rocks of the North Australian Craton (Maidment et al., 2020, 2022). Ages of 1877–1822 Ma for the metasedimentary rocks at Top Up Rise were interpreted as maximum deposition ages but deposition may be considerably younger. Zircon rims in both granitic gneiss and paragneiss samples at Top Up Rise record high-grade metamorphism and magmatism at 1625–1604 Ma (Kelsey et al., 2022). A migmatitic orthogneiss, sampled at about 605 m depth in this drillcore, yielded an age of 1875 ± 4 Ma, originally interpreted as magmatic crystallization (Wingate et al., 2022a), but reinterpreted as inherited xenocrysts as the rock is strongly peraluminous (Kelsey et al., 2022), and an age for metamorphism of 1612 ± 6 Ma (GSWA 243029, Wingate et al., 2022a). A migmatitic paragneiss, sampled at about 667 m depth in this drillcore, yielded 2801–1842 Ma detrital zircons, a maximum depositional age of 1876 ± 4 Ma, and an age for metamorphism of 1624 ± 13 Ma (GSWA 242032, Wingate et al., 2022b; Kelsey et al., 2022). From the current sample, in situ garnet Lu–Hf geochronology yielded an isochron age of 1696.5 ± 43.1 Ma (n = 37), and in situ biotite Rb–Sr geochronology yielded an isochron age of 1279.8 ± 54.2 Ma (n = 57) (Ribeiro et al., in prep.).

Petrographic description

The sample is a pelitic schist (Fig. 1) containing about 52% quartz, 31% muscovite, 15% biotite, 2% garnet, 1% chlorite and accessory apatite, ilmenite, zircon, monazite and (only in garnet) xenotime (Fig. 2; Table 1). The sample is compositionally layered, with alternating quartz-rich and muscovite-rich layers, and aggregates of biotite dispersed throughout (Figs 1–3). Quartz is abundant and occurs as aggregates with a seriate–polygonal to seriate–interlobate texture, internal subgrains, and grain size ranging from <100 µm to 3 mm, that help define the foliated layering. Biotite occurs as prismatic to acicular grains about 500 µm

to 1 mm long that define a well-developed foliation. Finer grained biotite (about 100 µm long) is common throughout. It has poorer grain shape and is more randomly oriented than coarser grained biotite, and it typically occurs together with some of the fine-grained muscovite. Coarse-grained muscovite (up to 1 mm long) is relatively rare and prismatic and helps to define the same fabric as biotite. Garnet occurs as rare rounded to elongate porphyroblasts (up to 1.5 mm long) wrapped by the micaceous fabric (Fig. 3). Some grains of garnet contain rounded to elongate inclusions of quartz that define a fabric subparallel to the main schist fabric. Biotite and xenotime occur as rarer inclusions in garnet.

Much of the sample consists of layered aggregates of fine-grained (about 100 µm long) muscovite, which help define the well-developed foliation. These layers range in width from about 50 µm to 1.0 – 1.5 mm. Some of these aggregates feature a fibrous, wavy matted texture that is reminiscent of fibrolitic sillimanite (Fig. 3). Chlorite is fine grained (up to about 150 µm long), has poor grain shape and occurs with fine-grained biotite and muscovite of similar size. Ilmenite occurs as rare, tiny (about 10–20 µm long) grains throughout the sample, but is more abundant where biotite occurs. Apatite occurs throughout the sample as elongate grains up to about 200 µm long.

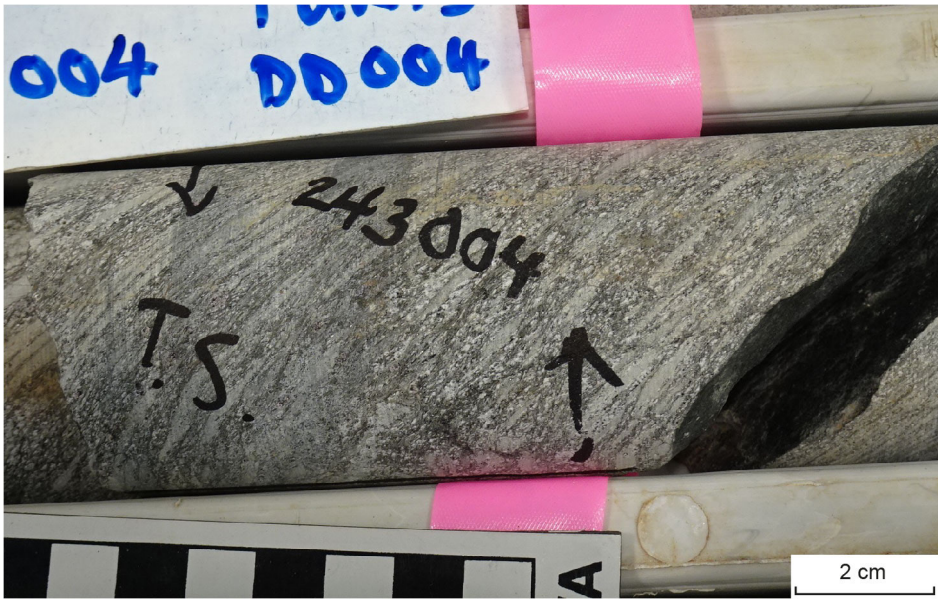

Figure 1. Drillcore image for sample 243004: garnet-bearing pelitic schist, Top Up Rise prospect

Table 1. Mineral modes for sample 243004: garnet-bearing pelitic schist, Top Up Rise prospect

Mineral modes	Qz	Ms	Bt	Grt	Sil[b]	Pl [b]	Chl	Ilm	Ap
Observed (vol%)[a]	52	31	15	2	–	–	1	<1	<1
Predicted (mol%)	52	31	15	2	–	–	1	<1	<1
@ 625 °C, 3.4 kbar	45	26	23	<1	2	1	–	<1	–
@ 675 °C, 6.5 kbar	44	31	20	2	<1	<1	–	<1	–
@ 725 °C, 8 kbar	41	27	17	4	2	–	–	<1	–

NOTES: (a) Trace monazite, zircon and xenotime also present in thin section
(b) Interpreted as formerly present, prior to retrogression
– not present

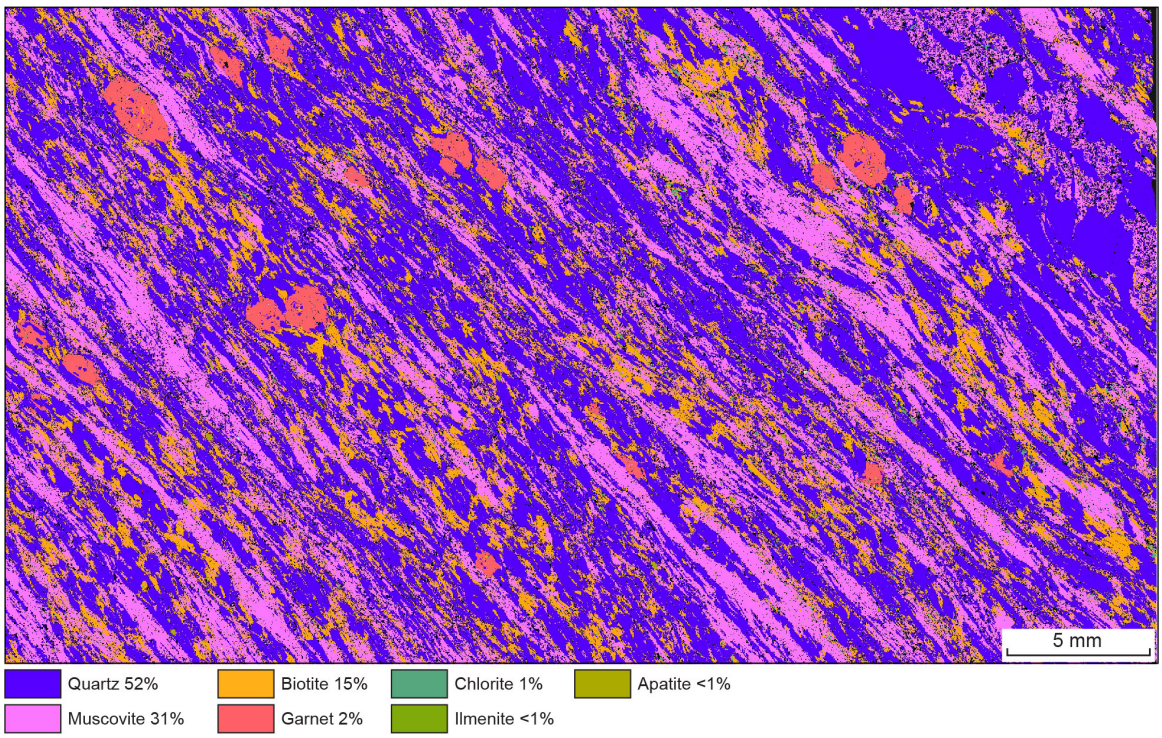

Figure 2. **TESCAN Integrated Mineral Analyser (TIMA) image of an entire thin section from sample 243004: garnet-bearing pelitic schist, Top Up Rise prospect. Volume percent proportions of major rock-forming minerals are calculated by the TIMA software**

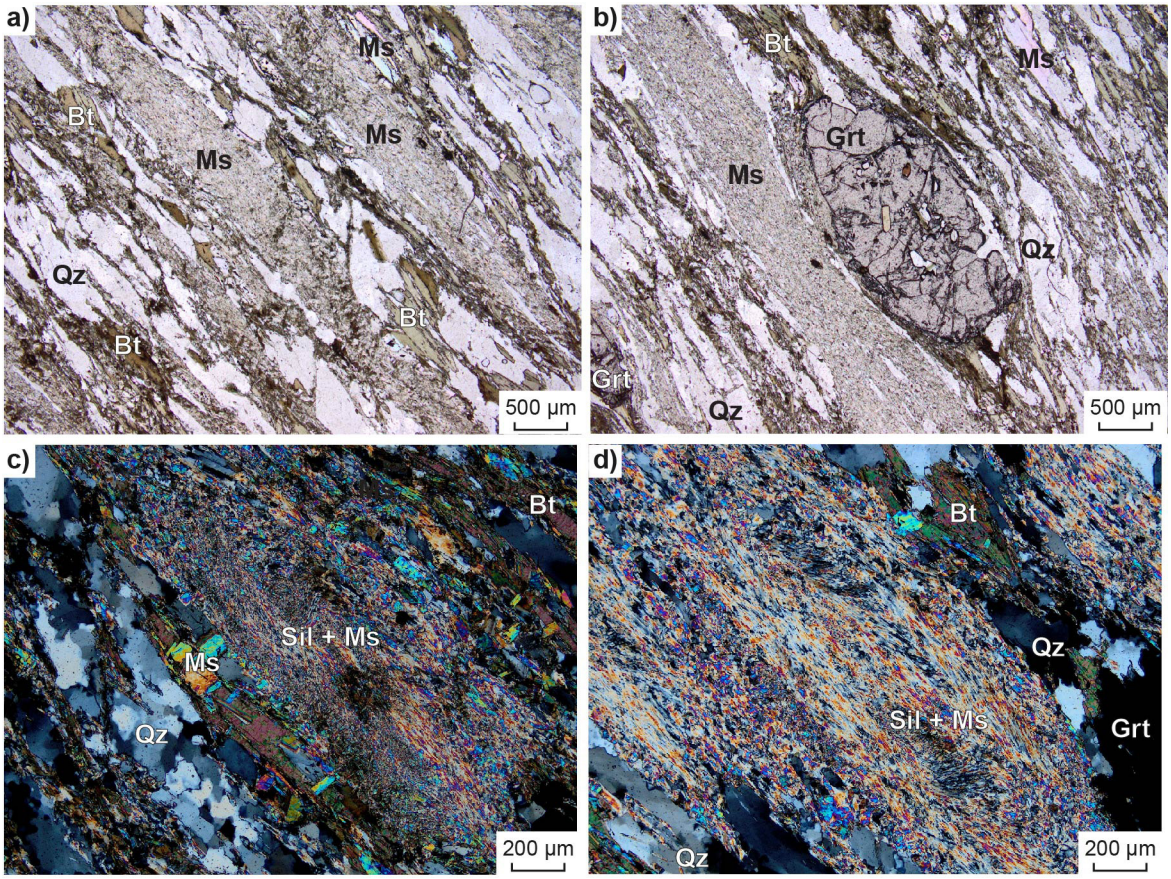

Figure 3. **Photomicrographs of sample 243004: garnet-bearing pelitic schist, Top Up Rise prospect. Abbreviations: Bt, biotite; Grt, garnet; Ms, muscovite; Qz, quartz; Sil, sillimanite**

Analytical details

The metamorphic evolution of this sample was investigated using phase equilibria, based on the bulk-rock composition (Table 2). The bulk-rock composition was determined by X-ray fluorescence spectroscopy, together with loss on ignition (LOI). FeO content was analysed by Fe^{2+} titration (as 85% of total Fe), and Fe_2O_3 calculated by difference. The modelled O content (for Fe^{3+}) was reduced slightly — to 11% from 15% — from the titration value as preliminary investigations using the titrated value led to the widespread stability of magnetite in pseudosections, which is not observed in the rock. The H_2O content was based on the measured amount of LOI, corrected for oxidation state. The bulk composition was corrected for the presence of apatite by applying a correction to calcium (Table 2). Thermodynamic calculations were performed in the MnNCKFMASHTO ($MnO–Na_2O–CaO–K_2O–FeO–MgO–Al_2O_3–SiO_2–H_2O–TiO_2–O$) system using THERMOCALC version tc340 (updated October 2013; Powell and Holland, 1988) and the internally consistent thermodynamic dataset of Holland and Powell (2011; dataset tc-ds62, created in February 2012). The activity–composition relations used in the modelling are detailed in White et al. (2014a,b). Compositional and mode isopleths for all phases were calculated using the software TCInvestigator (Pearce et al., 2015). Additional information on the workflow with relevant background and methodology are provided in Korhonen et al. (2020).

Mineral chemistry was acquired using a JEOL JXA-8530F Plus field emission electron microprobe (EPMA) at University of Tasmania, equipped with 5 wavelength-dispersive spectrometers. The EPMA is computer control by JEOL PC-EPMA and Probe Software Inc. 'Probe For EPMA' and 'Probe Image' software packages for all data acquisition and processing is used. Instrument operating conditions were 15 kV/10 nA with a 5 um defocused beam. Matrix corrections of Armstrong-Love/Scott φ(ρz) (Armstrong, 1988) and Henke MACs were used for data reduction. Mean Atomic Number (MAN) background correction (e.g. Donovan and Tingle, 1996; Donovan et al., 2016) was used over traditional 2 point background interpolation. Well-characterized natural minerals were used as standards for microprobe analytical sessions. Mineral compositions are provided in Appendix 1 as an accompanying electonic file (see **Links**).

Table 2. Measured whole-rock and modelled compositions for sample 243004: garnet-bearing pelitic schist, Top Up Rise prospect

XRF whole-rock composition (wt%)[a]												
SiO_2	**TiO_2**	**Al_2O_3**	**$Fe_2O_3^T$**	**FeO [b]**	**MnO**	**MgO**	**CaO**	**Na_2O**	**K_2O**	**P_2O_5**	**LOI**	**Total**
66.47	0.71	15.61	7.53	5.82	0.15	2.06	0.20	0.24	5.15	0.06	1.98	100.16
Normalized composition used for phase equilibria modelling (mol%)												
SiO_2	**TiO_2**	**Al_2O_3**	**O [c]**	**FeO^T [d]**	**MnO**	**MgO**	**CaO [e]**	**Na_2O**	**K_2O**	–	**H_2O [f]**	**Total**
67.97	0.55	9.40	0.32	5.79	0.13	3.14	0.13	0.24	3.36	–	8.97	100.00

NOTES: (a) Data and analytical details are available from the WACHEM database <http://geochem.dmp.wa.gov.au/geochem/>
(b) FeO content is by titration
(c) O content (for Fe_2O_3) modelled as 11% of total Fe
(d) FeO^T = moles FeO + 2 * moles O
(e) CaO modified to remove apatite: CaO(Mod) = CaO(Total) - (moles CaO(in Ap) = 3.33 * moles P_2O_5)
(f) H_2O content is LOI adjusted for oxidation state

Results

Metamorphic *P–T* estimates have been derived based on detailed examination of one thin section and a single bulk-rock composition. Care was taken to ensure that the thin section and the sample volume selected for whole-rock chemistry were similar in terms of featuring the same minerals in about the same abundances (Table 1), to minimize any potential compositional differences. The *P–T* pseudosection for sample 243004 was calculated over a *P–T* range of 2–10 kbar and 525–800 °C (Fig. 4). The H_2O-saturated solidus has a minimum stability of 670 °C at 4.2 kbar over the modelled *P–T* range. Garnet is stable over all of the modelled *P–T* range except the high-temperature – low-pressure corner. Sillimanite is stable at temperatures above 580 °C in a wedge-shaped region that expands in pressure with increasing temperatures. At higher pressure, staurolite (at lower temperatures) and kyanite (at higher temperatures), supersede sillimanite stability. Muscovite is stable over most of the diagram, excepting an approximately triangular region in the low-pressure – high-temperature corner. Biotite is stable everywhere across the modelled *P–T* range. Plagioclase is stable across the approximate *P–T* range of 2.0 – 6.7 kbar and 525–725 °C. Ilmenite is stable across the modelled *P–T* range and magnetite is stable in the low-pressure – high-temperature region.

Chlorite is stable at lower than about 585 °C and epidote is stable at lower than about 535 °C. Cordierite is stable at pressures below 4.5 kbar at 775 °C in an approximately triangular-shaped region.

Garnet is zoned and almandine rich (Appendix 2), with $Fe^{2+}/(Fe^{2+} + Mg + Mn + Ca)$ compositions lower at the outermost rim (0.69), highest in the 'inner rim' (0.78 – 0.79) and at 0.72 – 0.73 in the core (Appendix 1). Pyrope contents [$Mg/(Fe^{2+} + Mg + Mn + Ca)$] are low at the rim (0.02 – 0.04) and higher in the core (0.072 – 0.073). Spessartine contents [$Mn/(Fe^{2+} + Mg + Mn + Ca)$] are lower at the rim (down to 0.11) and higher in the core (0.175). Grossular contents [$Ca/(Fe^{2+} + Mg + Mn + Ca)$] are higher at the rim (up to 0.18) and lower in the core (0.02). Biotite is Fe rich (XFe = $Fe^{2+}/(Fe^{2+} + Mg)$ = 0.63 – 0.67) and has TiO_2 wt% 1.32 – 1.50 (0.08 – 0.09 cations per formula unit [pfu]). Fluorine and chlorine ions in biotite are 0.08 – 0.10 and 0.08 – 0.13 pfu, respectively (11 oxygen basis). Muscovite has paragonite content of 0.05 – 0.12. There is no clear difference in chemistry between coarse- and fine-grained muscovite. Chlorite is moderately Fe rich, with XFe ratios of 0.59.

Interpretation

Most or all fine-grained white mica, and some or all of the fine-grained biotite, is interpreted as post-peak retrogression of the sample. This white mica alteration is common in rocks from the Top Up Rise drillcore. Fine-grained muscovite is interpreted to have replaced former sillimanite and potentially plagioclase. Former sillimanite (now pseudomorphed) is interpreted on the basis that a wavy, fibrous texture occurs within some regions rich in fine-grained muscovite (Fig. 3). In addition, fresh sillimanite occurs in some other rocks from Top Up Rise drillcore, attesting to metamorphism occurring within sillimanite stability. Feldspar is not observed in the sample but plagioclase is interpreted as potentially formerly present on the basis of white mica (sericite) alteration of feldspar being common in rocks from Top Up Rise, and that the measured whole-rock geochemistry contains enough CaO to support the (former) presence of plagioclase, especially given that garnet has low modal abundance and is not CaO rich.

Rocks in the Top Up Rise drillcore are unmelted schists as well as melt-injected or partially melted 'wet' (mica-rich) migmatites. The high mica content of Top Up Rise rocks as well as the mix of unmelted and melted rocks suggests the rocks reached approximately the solidus but not much (if any) higher temperatures. Due to the degree of deformation of sample 243004, it is unclear whether it represents an unmelted schist or a partially melted migmatite. On these bases, the peak mineral assemblage is interpreted to be biotite–muscovite–garnet–sillimanite–ilmenite–quartz±plagioclase± melt (Fig. 4). This range of assemblages entails six fields in the P–T space, collectively stable over the P–T range 3.3 – 9.4 kbar and 580–780 °C. The sample was modelled using LOI corrected for oxidation state. This results in a wide field of coexisting H_2O and melt. Garnet mode, by TIMA, is ~0.018 (Fig. 2; Table 1), which would place the P–T conditions up towards the higher-P part of the peak fields (Appendix 2). The absence of kyanite from the sample – and from rocks at the Top Up Rise prospect – limits the maximum pressure for metamorphism. Garnet is not stable, and K-feldspar is stable, at pressures below the peak fields, which provide a minimum pressure constraint for metamorphism. Rocks at the Top Up Rise prospect did not exceed muscovite stability, providing a constraint on the maximum temperature.

Evidence of partial melting in the sample is unclear as leucosomes are not present at the scale of the hand specimen and melt films are not observed in the sample. Plagioclase is not present in the sample but is present in tiny amounts (≤ 0.13 modal vol. %) in the pseudosection below the solidus (Fig. 4). Such tiny amounts of plagioclase in the pseudosection but absence from the rock are considered unreliable constraints on the P–T conditions for the sample, but if taken at face value could indicate that peak P–T conditions for the sample were supradsolidus. Nevertheless, it is not possible to robustly decipher whether sample GSWA 243004 exceeded the solidus. It is unclear if later retrogression involving growth of fine-grained muscovite occurred during the same or a temporally different event. However, biotite Rb–Sr ages significantly younger than the garnet Lu–Hf and zircon U–Pb age data from Top Up Rise allow the possibility that retrogression was temporally separate from the amphibolite facies metamorphism.

There is limited petrological information to constrain any P–T path information. Peak metamorphic conditions are estimated at 3.3 – 9.4 kbar and 580–780 °C, with an apparent thermal gradient between 90 and 190 °C/kbar.

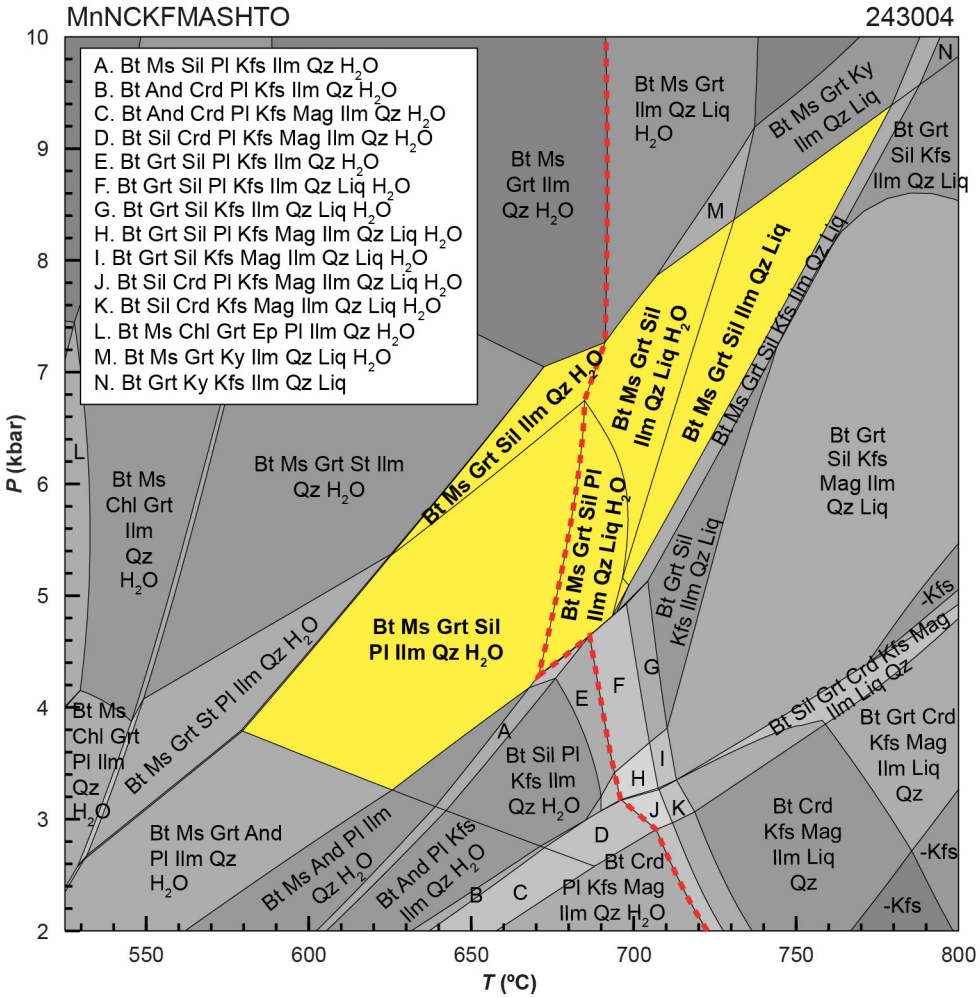

Figure 4. ***P–T*** **pseudosection calculated for sample 243004: garnet-bearing pelitic schist, Top Up Rise prospect. Assemblage fields corresponding to peak metamorphic conditions are shown in bold text and yellow shading. Red dashed line represents the solidus. Abbreviations: And, andalusite; Bt, biotite; Chl, chlorite; Crd, cordierite; Ep, epidote; Grt, garnet; H_2O, aqueous fluid; Ilm, ilmenite; Kfs, K-feldspar; Ky, kyanite; Liq, silicate melt; Mag, magnetite; Ms, muscovite; Pl, plagioclase; Qz, quartz; Sil, sillimanite; St, staurolite**

References

Armstrong, JT 1988, Quantitative analysis of silicates and oxide minerals: comparison of Monte-Carlo, ZAF and Phi-Rho-Z procedures *in* Proceedings of the Microbeam Analysis Society, *edited by* DE Newbury: San Francisco Press, San Francisco, p. 239.

Donovan, JJ amd Tingle, TN 1996, An improved mean atomic number background correction for quantitative microanalysis: Journal of Microscopy and Microanalysis, v. 2, no. 1, p. 1–7.

Donovan, JJ, Singer, JW and Armstrong JT 2016, A new EPMA method for fast trace element analysis in simple matrices: American Mineralogist, v. 101, no. 8, p. 1839–1853.

Holland, TJB and Powell, R 2011, An improved and extended internally consistent thermodynamic dataset for phases of petrological interest, involving a new equation of state for solids: Journal of Metamorphic Geology, v. 29, no. 3, p. 333–383.

Kelsey, DE, Wingate, MTD, Spaggiari, CV, Smithies, RH, Fielding, IOH, Lu, Y, Porter, JK and Finch, EG 2022, Crystalline basement beneath the eastern Canning Basin at the Top Up Rise prospect: Geological Survey of Western Australia, Record 2022/17, 15p.

Korhonen, FJ, Kelsey, DE, Fielding IOH and Romano, SS 2020, The utility of the metamorphic rock record: constraining the pressure–temperature–time conditions of metamorphism: Geological Survey of Western Australia, Record 2020/14, 24p.

Maidment, DW, Lu, Y, Phillips, C, Korhonen, FJ, Fielding, IOH, Wingate, MTD, Kirkland, CL, Murphy, R, Tilhac, R, Poujol, M and Zhao, J 2022, Geochronology of metasedimentary and igneous rocks in the Lamboo Province, Kimberley Region: reassessing collisional geodynamic models: Geological Survey of Western Australia, Report 215, 89p.

Maidment, DW, Wingate, MTD, Claoué-Long, JC, Bodorkos, S, Huston, D, Whelan, JA, Bagas, L, Lambeck, A and Lu, Y 2020, Geochronology of metasedimentary and granitic rocks in the Granites-Tanami Orogen: 1885–1790 Ma geodynamic evolution: Geological Survey of Western Australia, Report 196, 50p.

Marshall, D 2013, Final report for Exploration Incentive Scheme Funding DAG2012/00076897: E80/4427 Top Up project: Border Exploration Pty Ltd/Corazon Mining Limited: Geological Survey of Western Australia, Statutory mineral exploration report A099481, <www.dmirs.wa.gov.au/wamex>, 31p.

Pearce, MA, White, AJR and Gazley, MF 2015, TCInvestigator: automated calculation of mineral mode and composition contours for thermocalc pseudosections: Journal of Metamorphic Geology, v. 33, no. 4, p. 413–425, doi:10.1111/jmg.12126.

Powell, R and Holland, TJB 1988, An internally consistent dataset with uncertainties and correlations: 3. Applications to geobarometry, worked examples and a computer program: Journal of Metamorphic Geology, v. 6, no. 2, p. 173–204.

Ribeiro, BV, Kirkland, CL, Kelsey, DE, Reddy, S, Hartnday, MIH, Rankenburg, K, Liebmann, J, Korhonen, FJ and Clark in prep., In situ Rb-Sr reveals time–-strain pathway for shear zone mylonitic fabrics: Earth and Planetary Science Letters.

Scrimgeour, IR 2013a, Aileron Province: Chapter 12 *in* Geology and mineral resources of the Northern Territory, *compiled by* Ahmad M and Munson TJ: Northern Territory Geological Survey, Special Publication 5, p. 12:1 – 12:74.

Scrimgeour, IR 2013b, Warumpi Province: Chapter 13 *in* Geology and mineral resources of the Northern Territory, *compiled by* Ahmad M and Munson TJ: Northern Territory Geological Survey, Special Publication 5, p. 13:1 – 13:21.

White, RW, Powell, R, Holland, TJB, Johnson, TE and Green, ECR 2014a, New mineral activity-composition relations for thermodynamic calculations in metapelitic systems: Journal of Metamorphic Geology, v. 32, no. 3, p. 261–286.

White, RW, Powell, R and Johnson, TE 2014b, The effect of Mn on mineral stability in metapelites revisited: New a–x relations for manganese-bearing minerals: Journal of Metamorphic Geology, v. 32, no. 8, p. 809–828.

Wingate, MTD, Lu, Y, Fielding, IOH, Kelsey, DE and Spaggiari, CV 2022a, 243029: biotite–sillimanite orthogneiss, Top Up Rise prospect; Geochronology Record 1845: Geological Survey of Western Australia, 5p.

Wingate, MTD, Lu, Y, Fielding, IOH, Kelsey, DE and Spaggiari, CV 2022b, 243032: sillimanite–K-feldspar paragneiss, Top Up Rise prospect; Geochronology Record 1846: Geological Survey of Western Australia, 7p.

Appendix 2

Garnet compositional data from sample 243004: garnet-bearing pelitic schist, Top Up Rise prospect, obtained by electron probe microanalyser (EPMA). Full compositional data provided in Table 3. X(Fe^{2+}) = Fe^{2+}/(Fe^{2+} + Mg); p(Alm) = Fe^{2+}/(Fe^{2+} + Mg + Ca + Mn); p(Pyp) = Mg/(Fe^{2+} + Mg + Ca + Mn); p(Grs) = Ca/(Fe^{2+} + Mg + Ca + Mn); p(Sps) = Mn/(Fe^{2+} + Mg + Ca + Mn)

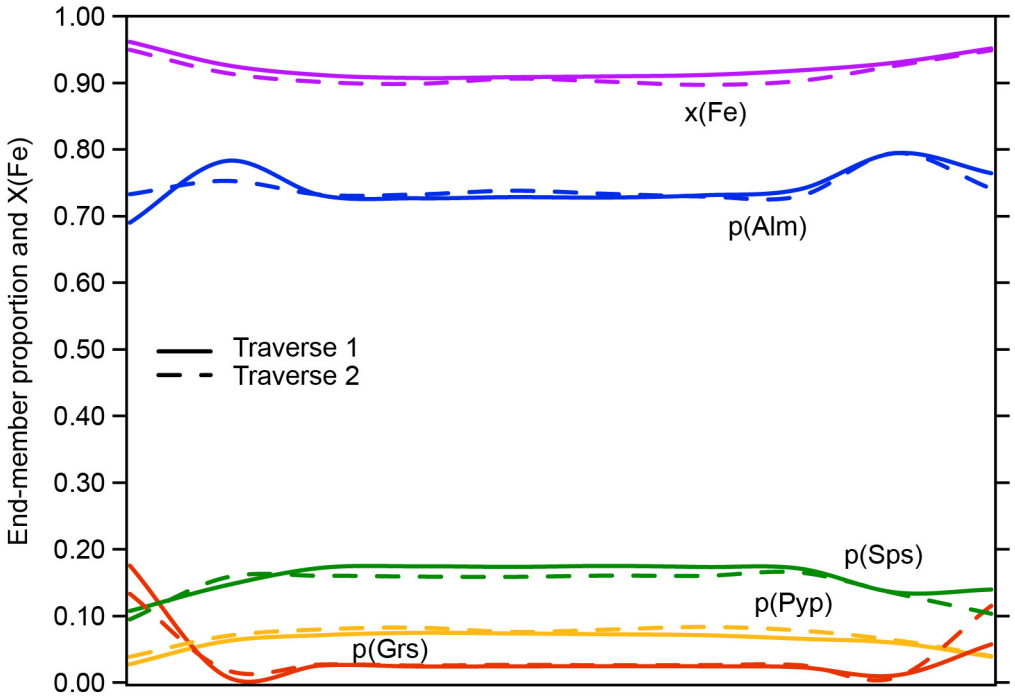

Appendix 3

Calculated phase volume percent modal proportion and solid-solution compositional data from sample 243004: garnet-bearing pelitic schist, Top Up Rise prospect. Labelled *P–T* pseudosection shown in Figure 4. See Appendices 1 and 3 for definitions of compositional variables

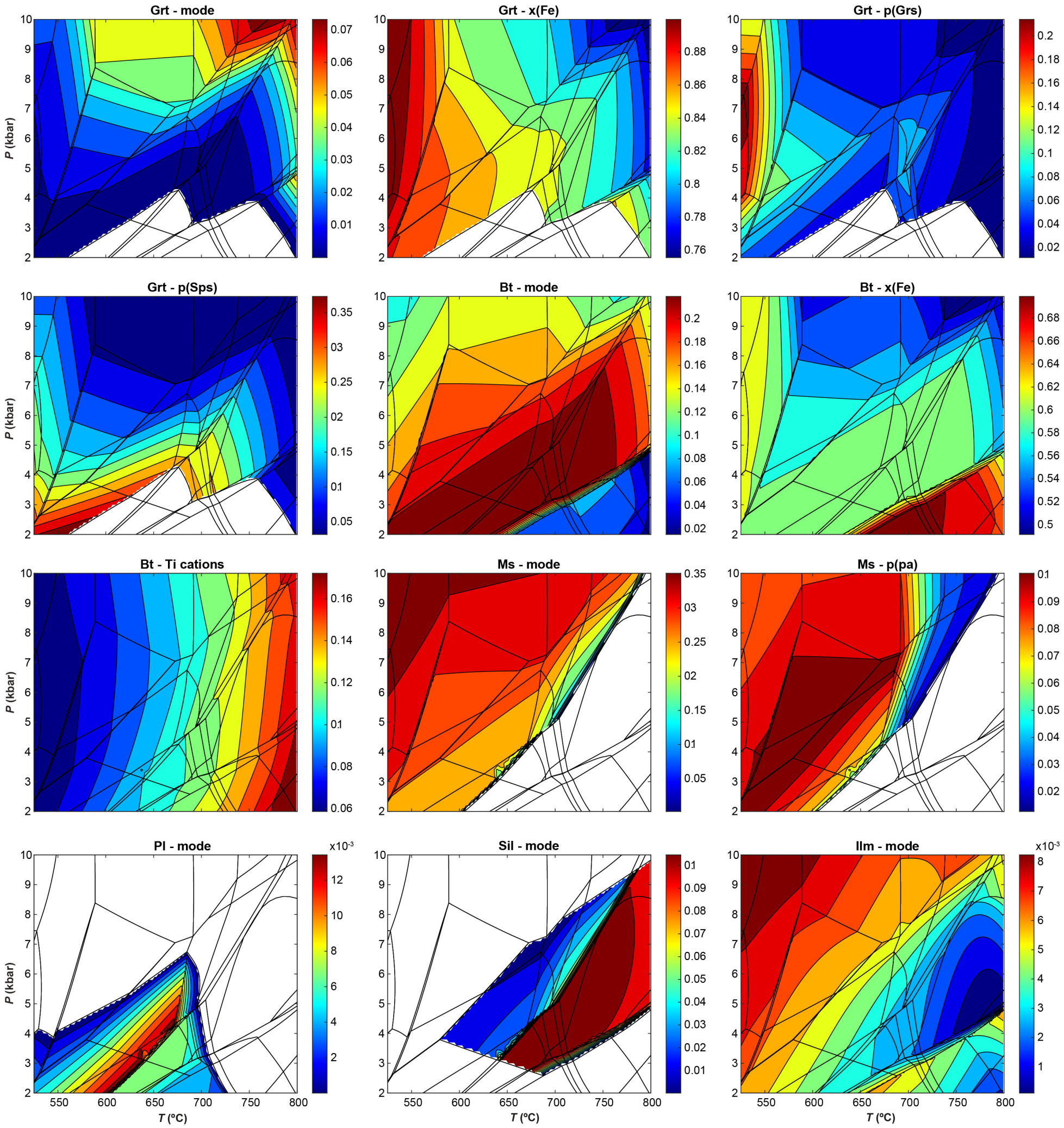

Links

Record 2020/14 The utility of the metamorphic rock record: constraining the pressure–temperature–time conditions of metamorphism

Appendix 1 (an accompanying electonic file on eBookshop)

Recommended reference for this publication

Kelsey, DE, Korhonen, FJ, Romano, SS and Spaggiari, CV 2022, 243004: garnet-bearing pelitic schist, Top Up Rise prospect; Metamorphic History Record 27: Geological Survey of Western Australia, 10p.

Data obtained: 22 August 2022

Date released: 9 December 2022

This Metamorphic History Record was last modified on 28 November 2022

Grid references in this publication refer to the Geocentric Datum of Australia 1994 (GDA94). All locations are quoted to at least the nearest 100 m.

WAROX is GSWA's field observation and sample database. WAROX site IDs have the format 'ABCXXXnnnnnnSS', where ABC = geologist username, XXX = project or map code, nnnnnn = 6 digit site number, and SS = optional alphabetic suffix (maximum 2 characters).

Isotope and element analyses are routinely conducted using the GeoHistory laser ablation ICP-MS and Sensitive High-Resolution Ion Microprobe (SHRIMP) ion microprobe facilities at the John de Laeter Centre (JdLC), Curtin University, with the financial support of the Australian Research Council and AuScope National Collaborative Research Infrastructure Strategy (NCRIS). The TESCAN Integrated Mineral Analyser (TIMA) instrument was funded by a grant from the Australian Research Council (LE140100150) and is operated by the JdLC with the support of the Geological Survey of Western Australia, The University of Western Australia (UWA) and Murdoch University. Mineral analyses are routinely obtained using the electron probe microanalyser (EPMA) facilities at the Centre for Microscopy, Characterisation and Analysis, UWA, at Adelaide Microscopy, University of Adelaide, and at the Electron Microscopy and X-ray Microanalysis Facility, University of Tasmania.

Digital data related to WA Geology Online, including geochronology and digital geology, are available online at the Department's Data and Software Centre and may be viewed in map context at GeoVIEW.WA.

Further details of geoscience products are available from:
Information Centre
Department of Mines, Industry Regulation and Safety
100 Plain Street
EAST PERTH WA 6004
Telephone: +61 8 9222 3459 | Email: publications@dmirs.wa.gov.au
www.dmirs.wa.gov.au/GSWApublications